Experimental critical dynamics of 3-methyl pyridine/D₂O mixtures without and with antagonistic salt

Henrich Frielinghaus [ORCID],[1,*] Purushottam S. Dubey,[1] Baohu Wu [ORCID],[1] Mary Odom [ORCID],[2] Feifei Zheng [ORCID],[3] Eunjoo Shin [ORCID],[4]
Piotr Zolnierczuk [ORCID],[2] Olaf Holderer [ORCID],[1] Stephan Förster,[5] and Theresia Heiden-Hecht[1]

[1]*Forschungszentrum Jülich GmbH, Jülich Center for Neutron Scattering JCNS-4 at MLZ, Lichtenbergstrasse 1, 85747 Garching, Germany*
[2]*Neutron Sciences Directorate, Oak Ridge National Laboratory (ORNL), P.O. Box 2008, 1 Bethel Valley Road, Oak Ridge,
Tennessee 37831, USA*
[3]*Department of Physics, Technical University of Munich, Munich, Germany*
[4]*Korea Atomic Energy Research Institute, 111, Daedeok-daero 989 beon-gil, Yuseong-gu, Daejeon 34057, South Korea*
[5]*Forschungszentrum Jülich GmbH, Jülich Center for Neutron Scattering JCNS-1, Neutronenstreuung und Materie IBI-8,
Leo-Brandt Strasse, 52425 Jülich, Germany*

We observed criticality in the structure and dynamics of a three-dimensional (3D) and two-dimensional (2D) Ising system consisting of 3-methyl pyridine (3MP)/D₂O without and with antagonistic salt. We could describe both dynamic criticalities by the Kawasaki crossover function. The dynamic critical exponent was $z = 0.063 \pm 0.020$ and 0.005 ± 0.019 for three and two dimensions, which confirms earlier observations in the 3D case and confirms expectations in the 2D case. The amplitudes of the critical dynamics are governed by the bare viscosities experimentally, and by the coefficient R theoretically [the latter is proportional to $(4 - d)^{-1}$ with the dimensionality d]. This finding is in accordance with the lubrication effect [N. Gov, A. G. Zilman, and S. Safran, Phys. Rev. E **70**, 011104 (2004)], which is also connected to lamellar systems of the Brazovskii criticality [M. Gvaramia *et al.*, Colloid Polym. Sci. **297**, 1507 (2019)]. This lubrication effect is tightly connected to a laminar flow enforced by the domain structure, and it also holds for our 2D Ising system. The experimental techniques employed were small-angle neutron and x-rays scattering for the static criticality, and dynamic light scattering and neutron spin echo spectroscopy for the critical dynamics. Furthermore, the criticality of the viscosities was measured.

I. INTRODUCTION

It is a general, highly interesting question as to what impact confinement has on fluid mobility. The latest developments of electrolytes are based on water with polymers and lithium salts, which may display electrochemical changes [the solid electrolyte interphase (SEI)] close to the electrode [1]. Apart from chemical modifications, the physical transport properties, i.e., the electrolyte mobility, and the ion transport properties at the interface are responsible for the maximum current at which the batteries can be charged or discharged [2]. Also in fuel cells and electrolyzers, the proton mobility in the porous membrane is important for the performance of the whole cell [3].

The confinement can be exerted by a single-sided wall or nanopores. For polymers, we find higher and lower mobility in nanopores [4]. Ionic liquids display a higher mobility in mild confinement of nanopores [5]. Single-sided confinement may increase or decrease the mobility [6]. Due to the charges and hydrophobic moieties, the exact structure of the pore surface is of minor interest [7]. Confinement on the single molecule scale is possible in carbon nanotubes [8], but it is beyond the scope of the current manuscript.

For the classification of mobility changes under confinement, the fluid type also has an important impact. The Brazovskii class of fluids [9–11]—to which microemulsions are also counted—display a lubrication effect [12] when exposed to single-sided planar walls. Here, the otherwise random orientation of alternating domains is oriented in a lamellar arrangement of domains close to the walls [13]. The lamellae allow a sliding of the domains against each other and all flow fields stay laminar, which means a higher mobility of the fluid due to a single-sided planar confinement. A detailed study about microemulsions and crude oils exposed to planar surfaces from clay particles can be found in the literature [14]. Also diblock copolymer blends display facilitated flow in a shear field between parallel plates [15]. To our knowledge, the critical dynamics of the Brazovskii type of fluids has only been studied to a small extent.

A complementary type of fluid is the binary Ising fluid [16,17]. It lacks amphiphilic materials, and so domains are only an issue of critical composition fluctuations close to the phase boundary. So the size of domains is directly influenced by the criticality. One example is the mixture of 3-methyl-
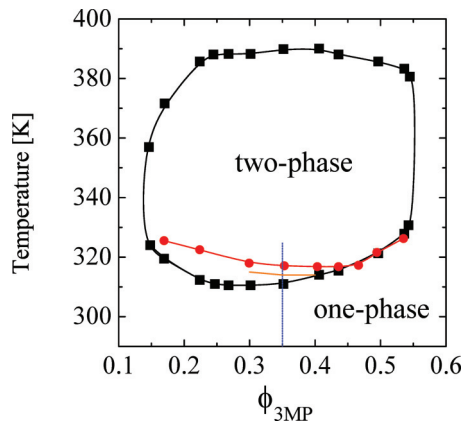
FIG. 1. The experimental phase diagram from Sadakane [18] of the 3MP/D_2O system without (black) and with (red) antagonistic salt sodium tetraphenylborate (5 mmol/L). The system is one-phase at lower temperatures. The reentrant phase diagram describes demixing at intermediate temperatures, and the one-phase range at elevated temperatures is omitted in our study. The blue line indicates the 3MP concentration of this paper, where we only vary the temperature. The orange line indicates the Lifshitz line of the system with antagonistic salt: At low temperatures, an additional lengthscale appears from the charge density waves, which then is lost in the narrow temperature range close to the phase boundary of demixing.

pyridine (3MP, or 3-picolin) and heavy water (D_2O) among others [18,19]. But also single-component supercritical gases are well-studied examples [20]. They all fall in the case of three-dimensional Ising criticality, which is usually confirmed by the critical exponents of the susceptibility or the correlation length. A recent study of the Widom line [21] focuses on special properties of supercritical CO_2 that is not the focus of the current study.

A rather complicated system is obtained from the 3MP/D_2O system when adding antagonistic salt (or also ionic surfactants). In Fig. 1 we display the experimental phase diagram of 3MP/D_2O without and with antagonistic salt sodium tetraphenylborate. The phase boundary is lifted by the addition of antagonistic salt by about 6 K (this seems to be a general impact of salt additives [22]). The 3MP concentration of this paper is highlighted by the vertical blue line. A Lifshitz phase diagram is found experimentally when adding antagonistic salt [18], because now an Ising system meets the amphiphilicity from the additive, and so, in principle, a Brazovskii Hamiltonian applies [23,24]. This criticality is found at lower temperatures and is indicated by a very weak peak in the SANS patterns. At a narrow temperature range close to the critical temperature, the system loses the additional lengthscale of the Lifshitz criticality, and experiments display a two-dimensional Ising criticality for the composition fluctuations [18] that seems to persist even at lower temperatures. This is due to the very low concentrations of additive: The charge-density waves happen on much larger lengthscales [23–25] (i.e., the additional lengthscale of the Lifshitz criticality) and so it must be the wave-fronts that propagate through the material and impinge a 2D confinement to the dominating composition fluctuations. A sketch for this situation is depicted in Fig. 2. Most of the ions are aligned
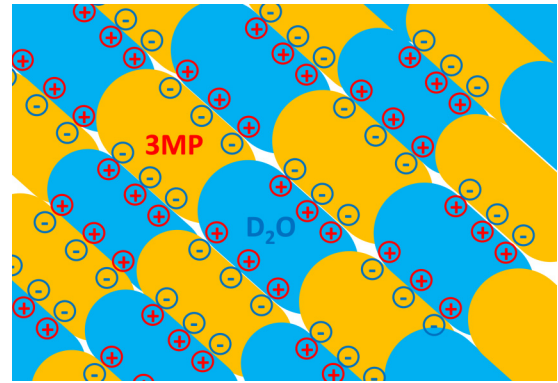

FIG. 2. A sketch for the charge density waves in the 3MP/D_2O mixture with antagonistic salt. The domains are colored orange for 3MP and blue for D_2O. The respective ions are indicated by circles, and their charge is inside the circles.

in planes between the domains of 3MP and D_2O. The charge density waves lead to breathing modes of the different encapsulated domains. They propagate perpendicular to the planes, and their typical wavelengths are much larger than the domain sizes themselves. When the system becomes more critical, the domain sizes grow and the concentration of charges at the domain surfaces becomes higher. But the exact mechanisms are still under debate. At high salt concentrations, this splitting of lengthscales does not occur anymore [19,26–28].

The aspect of dynamic asymmetry was raised for mainly polymer/solvent systems by Tanaka [29,30]. However, the viscosities of 3MP and D_2O are very similar [31] and so dynamic asymmetry can be safely neglected. This is also reflected by a strong coupling of motions between the two components as found by quasielastic neutron scattering experiments [32]. For the sake of curiosity, we would like to add that 2D and 3D Ising criticality can also be found in magnetic systems [33], however long-range dipolar interactions cause complications and so these systems are not really comparable to our work.

In this manuscript, we describe the criticality of a 3D and 2D Ising system formed by 3MP and D_2O without and with antagonistic salt. We describe the static criticality, i.e., the susceptibility and the correlation length, and then we continue with the critical dynamics measured by spectroscopic scattering experiments. The results are discussed in the context of current literature, and a conclusion is drawn.

II. THEORY

We briefly describe the static criticality of 3D and 2D Ising systems for the forward scattering $I(Q \to 0)$ and the correlation length ξ of a small-angle scattering experiment. Here, the scattering intensity $I(Q)$ is observed as a function of the scattering vector Q, which is proportional to the scattering angle θ at small angles according to $Q = (4\pi/\lambda)\sin(\theta/2)$. It carries the reciprocal unit of a length from the wavelength λ. So, an intensity peak at Q^* can be directly related to a real space length $\ell = 2\pi/Q^*$, which is also known as the Bragg relation. For small Q the scattering intensity of an Ising system

TABLE I. The universal critical exponents of the 2D and 3D Ising behavior in the one-phase system.

Exponent	2D Ising	3D Ising
γ	7/4	1.239
ν	1	0.627

is described by the Ornstein-Zernicke law [34]:

$$I(Q) = \frac{I(Q \to 0)}{1 + \xi^2 Q^2}. \tag{1}$$

The forward scattering $I(Q \to 0)$ also plays the role of susceptibility. Its criticality close to the critical point (in the one-phase region) takes the following temperature dependence:

$$I(Q \to 0) = I_0 \tau^{-\gamma}. \tag{2}$$

I_0 is the critical amplitude, and τ is the reduced temperature, i.e., $\tau = |T - T_C|/T_C$. The critical exponent γ describes how quickly the scattering intensity diverges at the critical temperature T_C. For compositions that are slightly different from the critical composition, the spinodal temperature T_S takes the role of the critical temperature in a temperature scan experiment. For the correlation length ξ, a similar behavior is found:

$$\xi = \xi_0 \tau^{-\nu}. \tag{3}$$

The critical amplitude is ξ_0 and the critical exponent is called ν. For 2D and 3D Ising systems, the critical exponents are universal and are listed in Table I.

While the static criticality, i.e., the susceptibility and the correlation length, is well reported for the 3MP/D_2O system with/without additive, the criticality of the transport properties, i.e., the viscosity and the diffusion constant, has not been reported so far. In classical 3D Ising systems, this has been analyzed experimentally [35,36] and theoretically [37,38]. So, for instance, the long-range diffusion constant scales as

$$D = \frac{k_B T}{6\pi \eta \xi} = \frac{k_B T}{6\pi \eta_b Q_0^z \xi^{1+z}}. \tag{4}$$

Here, the criticality of the viscosity is split off by the term $(Q_0 \xi)^z = \tau^{-x}$ from the bare viscosity η_b that displays an Arrhenius or Vogel-Fulcher temperature behavior (see the discussion below). The critical amplitude Q_0 is determined by the critical amplitude of the temperature dependence of the correlation length according to $Q_0 = \xi_0^{-1}$. The exponent $z = x/\nu$ can be split in the critical temperature dependence of the viscosity and the correlation length. Experimentally and theoretically [36,39], it was confirmed that $x = 0.042$ and so $z = 0.067$.

The 2D Ising criticality of the transport phenomena becomes obscure because of the Pomeau logarithmic divergence. At short times, the diffusion describes a random walk still, while at longer times the diffusion crosses over to a different power law [38]. So strictly speaking, the transport of the 2D Ising case would be governed by different physics. However, we could measure the classical diffusion of the 3MP/D_2O system with additive. From earlier estimations

[40], the exponent z would be governed by criticality of the heat capacity and the correlation length, i.e., $z = \alpha/\nu$, and so in the 2D Ising case this exponent would change to $z = 0$ due to the logarithmic divergence of the heat capacity in two dimensions with $\alpha = 0$. More details will be given in the discussion below. An alternative argument was given by Hohenberg and Halperin [41]. They derived for the diffusion constant $D = \lambda/\chi \sim \xi^{2-d}$ [Eq. (2.22)], with λ being the thermal conductivity and χ the susceptibility.

Using scattering experiments, the diffusion can be measured on long and shorter lengthscales. The diffusion then displays a crossover behavior from the classic hydrodynamic diffusion [as Eq. (1)] to the critical diffusion where the critical fluctuations dominate the behavior. The diffusion constant now reads [37]

$$D = \frac{k_B T}{6\pi \eta \xi} R\Omega(Q\xi). \tag{5}$$

The lengthscale dependence ($X = Q\xi$) is now included in the crossover function:

$$\Omega(X) = \Omega_K(X)(1 + b^2 X^2)^{z/2}, \tag{6}$$

where the Kawasaki crossover function reads [42]

$$\Omega_k(X) = \frac{3}{4X^2}[1 + X^2 + (X^3 - X^{-1})\arctan(X)]. \tag{7}$$

In the 3D Ising case, the coefficients read $R = 1.02$ and $b = 0.55$.

III. MATERIALS

The chemicals 3-methyl-pyridine (3MP, 99.5% purity) and the antagonistic salt sodium tetraphenylborate (NaBPh4, 99.5% purity) were purchased from Sigma Aldrich, Taufkirchen and used as received. Heavy water (D_2O, 99.8% purity) was purchased from Armar Chemicals, Döttingen and used as received. The 3MP/D_2O mixtures were mixed by volume (35%vol 3MP). Using a balance and pipettes, the molarity of 6 mmol/L of the antagonistic salt was adjusted. The critical temperatures of 311.5 and 315.8 K of the 3D and 2D Ising systems could vary slightly with different experimental setups (± 1.5 K) due to differing temperature gradients while the statistical precision was much better than the worst case of ± 10 K. The systems are lower critical solution temperature (LCST) systems.

IV. EXPERIMENTS

SANS experiments have been performed at the instrument 18M-SANS at the research reactor HANARO, Republic of Korea. The neutron wavelength was $\lambda = 5$ Å, and 10 Å detector distances of 3.1 and 9.1 m were used. The neutron velocity selector had a wavelength spread of $\pm 15\%$ (FWHM). The intensities were calibrated using the secondary standard of porous silica. All data were corrected for background scattering and radially averaged to obtain intensities as a function of the scattering vector $Q = (4\pi/\lambda)\sin(\theta/2)$ for isotropic scattering, and θ being the geometric scattering angle.

SAXS experiments were performed by a laboratory based SAXS/WAXS/USAXS beamline KWS-X (XENOCS
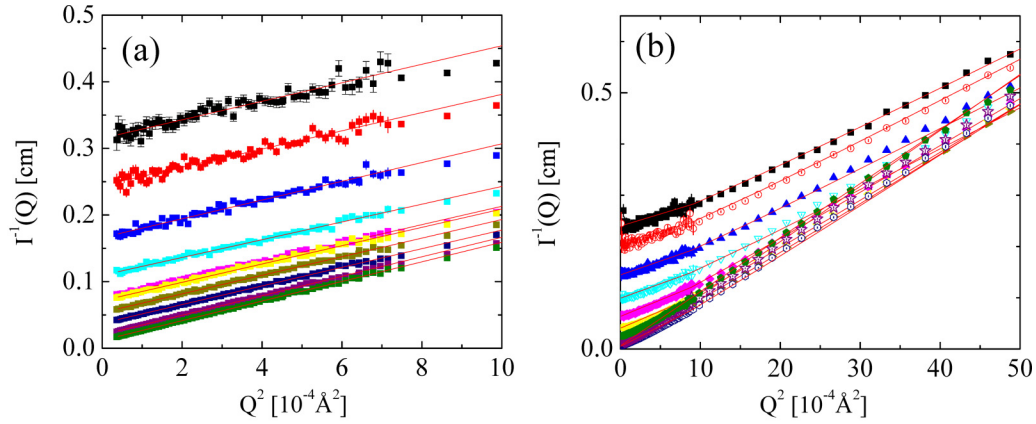
FIG. 3. (a) Zimm plot of the 3D Ising system obtained from SANS. The lower density of data points at higher Q results from the second, shorter detector distance. The temperatures were (from top to bottom) 293.2, 296.2, 299.2, 302.2, 304.2, 305.2, 306.2, 307.2, 308.2, and 309.2 K. (b) Zimm plot of the 2D Ising system obtained from SANS. To cover the two different slopes of the measurement, the considered Q-range was extended. The temperatures were (from top to bottom) 293.2, 296.2, 299.2, 302.2, 305.2, 307.2, 311.2, 313.2, 314.2, and 315.2 K.

XUESS 3.0 XL Garching) at JCNS MLZ. The x-ray source is a D2+ MetalJet (Excillum) with a liquid metal anode operating at 70 kV and 3.57 mA with Ga $K\alpha$ radiation (wavelength $\lambda = 1.314$ Å). Solution samples were measured in a glass capillary (1.5 mm ID) that was kept from 20 and 45 °C in a temperature-controlled Peltier stage. The sample to detector distances (SD) were 0.65 and 1.691 m, which cover the scattering vector q range from 0.005 to 0.35 Å^{-1}. The scattering patterns were obtained with a short exposure time 600 s and repeated six times. The SAXS patterns were normalized to an absolute scale, corrected for background, and azimuthally averaged to obtain the intensity profiles. Details about the instrument can be found on the producer's web page.

DLS measurements have been performed at an LS Spectrometer from LS Instruments [43]. The wavelength was $\lambda = 660$ nm with a negligible wavelength spread. Samples were measured in cylindrical quartz cuvettes with a diameter of 5 mm and a wall thickness of 0.4 mm. Rectangular cuvettes were used for reducing the laser path length with the thickness of 1.25 mm and an optical path of 10 mm (by measuring close to the corner at a scattering angle of 90°). During the measurements, the cuvettes were immersed in a temperature-controlled bath of the index matching solvent decalin. The scattering angles were rendered from 30° to 135° in 5° steps. Each collected spectrum was repeated three times in order to determine statistical errors and spikes from dust particles. Data with larger statistical errors than 10% were neglected in the following.

NSE measurements have been performed at the Neutron Spin Echo Spectrometer NSE at the Spallation Neutron Source SNS in Oak Ridge, USA [44]. Neutron wavelength bands of $\lambda = 3$–6 and 6–9 Å have been used. For resolution reference, elastic scatterers (Al$_2$O$_3$ and grafoil) were measured. The reduction of the data was performed by the new software DrSpine [45], and so correlation functions were obtained in a Fourier time space from 0.1 to 50 ns and Q-space from 0.04 to 0.27 Å^{-1}. All samples were measured in Hellma quartz cells with a thickness of 2 mm in the standard sample environment with temperature control by a thermalized air

stream via the Thermojet ES (SP Scientific, Warminster, PA, USA). Intermediate scattering functions were measured between 20 and 36 °C for the 3D Ising system in 10 temperature steps and 20 and 40 °C for the 2D Ising system in eight temperature steps.

Viscosity measurements have been performed on a Lovis 2000 M/ME rolling-ball viscometer from Anton Paar, Graz, Austria following Höppler's falling ball principle. This method is highly accurate for viscosities being not very different from water as in our case. Apart from viscosities, the instrument also determines the density with the DMA M density meter option using the U-tube technology based on the Pulsed Excitation Method. Details can be found on the producer's webpage.

V. RESULTS

We present the SANS data of the 3D Ising system as Zimm plots [Fig. 3(a)], where the forward scattering $I(0)$ and the correlation length ξ can be obtained from the linear regression as $I^{-1}(Q) = I^{-1}(0)(1 + \xi^2 Q^2)$. One can see that the system becomes critical with increasing temperature as the forward scattering $I(0)$ increases. The correlation length behaves similarly, as the slope in the Zimm plot only varies slightly. The same measurements have been performed as SAXS experiments, which we summarize in the Supplemental Material [46].

We also present the SANS data of the 2D Ising system as Zimm plots [Fig. 3(b)] because the influence of the amphiphilic additive is relatively small. The scattering function proposed by Onuki and Kitamura [23] reads $I^{-1}(Q) = I^{-1}(0)[1 + \{1 - \kappa^2/(1 + \lambda_D^2 Q^2)\}\xi^2 Q^2]$, with κ deviating slightly from 1, and the Debye length $\lambda_D = 39.25$ Å. The theory is based on a Ginzburg-Landau approach that describes preferential solvation around the charges of NaBPh4. Close to the critical point, strong electrostriction is described. Within the Born approximation, the Ornstein-Zernicke scattering diverges, and multiple scattering effects renormalize the scattering function. All reciprocal scattering curves display
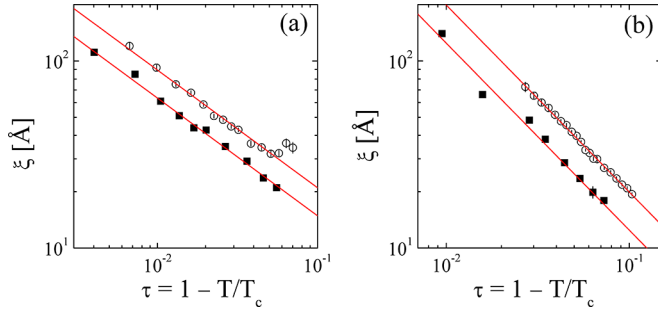
FIG. 4. (a) The criticality of the correlation length ξ as a function of the reduced temperature τ of the 3D Ising system determined by SANS and SAXS. Due to temperature gradients and possibly not complete background subtraction, the SAXS data display deviations in terms of the critical temperature and absolute values of ξ. The critical exponent was set to 0.629. (b) The criticality of the correlation length ξ as a function of the reduced temperature τ of the 2D Ising system determined by SANS. For the solid line, the critical exponent was set to 1.00. For all plots, the error bars are of the symbol size as one can see from the error bars in the open symbols of the SAXS measurements.

a smaller slope at smaller Q compared to larger Q. This is an effect of the nonzero value κ. The correlation length is represented by the slope at higher Q in the range of the presented Zimm plot, while the low-Q end originates from the charge density waves. The detailed results from our analysis are presented below. Again, SAXS results are summarized in the Supplemental Material [46].

We present the criticality of the the correlation length of the 3D Ising system from SANS and SAXS data in Fig. 4(a), and we refer the reader to the Supplemental Material [46] for the extrapolated forward scattering (S2a). The measured data comply with fixed critical exponents of $\gamma = 1.239$ and $\nu = 0.629$. Details for the fitting parameters are found in Table II. As the forward scattering and the correlation length take quite large values close to the critical temperature, we can state that the system is quite close to the critical point and the phase transition is quasi-second-order. It is evident that the SAXS data do not agree with the SANS data. The reasons for the deviations are the incomplete background subtraction and temperature gradients of the sample holder for the capillaries in vacuum. The construction of the SANS sample holder is much more closed around the banjo cuvettes, so the temperature gradients are to a large extent avoided. The background in SANS experiments can also be well determined. So in the

TABLE II. The parameters of the static criticality measured by SANS for the 3D Ising and the 2D Ising systems.

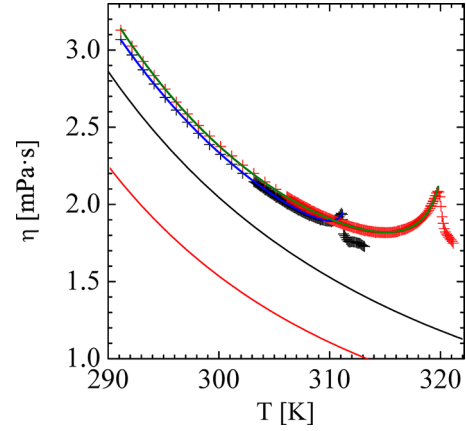| Parameter	3D Ising	2D Ising
I_0 (cm^{-1})	0.0878 ± 0.0026	0.0398 ± 0.0024
T_C (K)	309.96 ± 0.25	315.78 ± 0.62
γ	1.239 fixed	1.75 fixed
ξ_0 (Å)	11.54 ± 0.34	1.300 ± 0.040
T_C (K)	310.06 ± 0.24	316.40 ± 0.47
ν	0.629 fixed	1.00 fixed

FIG. 5. The measured viscosities of the 3D Ising (black) and 2D Ising (red) system with model fits according to Eq. (8) (blue and green). The solid lines (black and red) below indicate the bare viscosities η_b.

following, we will only discuss the static criticality measured by SANS.

We also present the criticality of the correlation length of the 2D Ising system from SANS and SAXS data in Fig. 4(b) (the forward scattering can be found in the Supplemental Material [46], Fig. S2b). The measured data comply with fixed critical exponents of $\gamma = 1.75$ and $\nu = 1.00$. Details for the fitting parameters are found in Table II. It is evident that the SAXS data do not agree with the SANS data for the same reasons as mentioned before. The charge density wave influences the forward scattering $I(Q = 0)$ at low temperatures, i.e., far away from the critical temperature. Here, also the κ-values of the SAXS measurements are considerably larger than 1 (see the Supplemental Material [46], Fig. S3). The temperature shift of the 2D Ising systems with respect to the 3D Ising system can be explained by the ionic nature of the salt [22]. All the static criticality experiments serve to determine the critical amplitude ξ_0 of the correlation length. We preferred the SANS experiments because we believe the systematic experimental errors are much lower compared to SAXS.

The viscosities of the 3D and 2D Ising system are presented in Fig. 5. Earlier published measurements did not describe any criticality [31]. At higher temperatures, the Vogel-Fulcher [47,48] dependence η_b dominates while the criticality dominates towards lower temperatures. The data at the lowest temperatures below the "divergence" of the viscosity are just presented for reference. The solid lines present the fitted curves to the theoretical expression as follows:

$$\eta = \underbrace{\eta_0 \, \exp\left(\frac{A}{T - T_0}\right)}_{\eta_b} \cdot \left(\frac{T_C - T}{T_C}\right)^{-x_\eta}. \qquad (8)$$

Both systems could be described successfully with this theory. The resulting parameters are presented in Table III. The bare viscosities are presented as solid lines in Fig. 5. For the 3D Ising system, we use the full dependence of the viscosity $\eta = \eta_b (Q_0 \xi)^y$ by just rewriting the criticality in terms of the correlation length ξ with $y = x_\eta / \nu$ and $Q_0 = \xi_0^{-1}$. So we stress that the original measured range of the viscosity

TABLE III. The parameters to describe the viscosity of the 3D and 2D Ising system.

Parameter	3D Ising	2D Ising
η_0 (mPa s)	0.0231 ± 0.0113	0.0138 ± 0.0036
A (K)	643.9 ± 127.2	629.5 ± 61.0
T_0 (K)	156.4 ± 12.6	166.3 ± 5.7
T_C (K)	311.5 ± 0.3	320.8 ± 0.1
x_η	0.040 ± 0.005	0.162 ± 0.006

is applied in terms of an interpolation, which means that the statistical errors of 0.2% apply independent of the larger statistical errors of the fit parameters. For the 2D Ising system, we apply the same method, but—as we will see—the exponent y from the spectroscopic scattering experiments is different from the one derived from the viscosity measurements with $x_\eta = 0.162$. Other binary systems could possibly confirm this exponent experimentally [49] that theoretically could be even larger ($x_\eta = 0.33$) [50]. The charge density waves impose a lamellar structure on the 2D Ising system, which supposedly is aligned in the shear field. So the criticality of the viscosity has a different meaning from the one used for the scattering experiments. The statistical error of the bare (Vogel-Fulcher) viscosity η_b is only in the range of 0.5% for the 2D Ising system when being used in the interpretation of the dynamic scattering experiments. We also stress that the critical temperature of the 2D Ising system is shifted to higher temperatures by about 4 K (if compared to Table I). Thus, the shear field seems to stabilize the one-phase region. The main point of this observation is that the bare viscosity is unchanged by this little temperature shift of the critical temperature and still can be used for the analysis of the dynamic scattering experiments. We also want to stress that critical viscosity measurements have been conducted before [51].

The densities measured in parallel with the same instrument displayed a first-order phase transition, but they are only shown in the Supplemental Material [46] of this manuscript. So the experimental system did not completely hit the critical composition, but it came very close. The transition temperatures of the density measurements completely agree with the viscosity measurements.

The raw data of DLS measurements at 20 °C are depicted in Figs. 6(a) and 6(b). We can see that the 3D Ising system could be well described using a single exponential function. The small shoulder at $Q = 0.000\,49$ Å^{-1} was a rare event for the lowest Q and lower temperatures. So we generally ignored this very weak second process, which might be the second slow mode being dominated by thermal diffusivity [52]. Only hydrophobic impurities may amplify a small mode dramatically [53,54] (and clathrates have also been found [55]). The 2D Ising system needed to be described by two exponential functions. Since the faster times are similar in both measurements, we addressed them for the composition fluctuations of 3MP and D_2O, while we connected the slower times to the charge density waves, which are much stronger than the thermal diffusivity modes of the 3D system. We omitted this contribution only if the second process was insignificant in the model fit. For the 2D Ising system, we observed clear indications of multiple scattering (the laser power was reduced by the instrument, and the last five temperatures displayed elevated, Q-independent diffusion constants). So we remeasured the sample in a rectangular cell with shorter light paths at 90° scattering angle. We obtained a general correction factor of 0.7 for all diffusion constants, and the last five temperatures were adjusted to have a constant master curve (see Fig. 8) for all DLS data. A general correction of DLS data with multiple scattering by constant factors was motivated in Ref. [56].

With NSE, the intermediate scattering function is measured similar to DLS, but on molecular lengthscales and timescales. A review and the capabilities of NSE are, for example, described in Ref. [57]. The raw relaxation curves of the NSE measurements at 20 °C are displayed in Figs. 7(a) and 7(b). All spectra were analyzed using a single (nonstretched) exponential to describe each relaxation curve. An amplitude slightly smaller than 1 had to be used. Both the 3D Ising and 2D Ising system stayed in the same range of relaxation times, indicating the small perturbation by the antagonistic salt.

VI. DISCUSSION

The summary of the spectroscopic scattering experiments is displayed in Fig. 8. Here, all scaled diffusion constants are collected for the 3D Ising and 2D Ising system. The data of
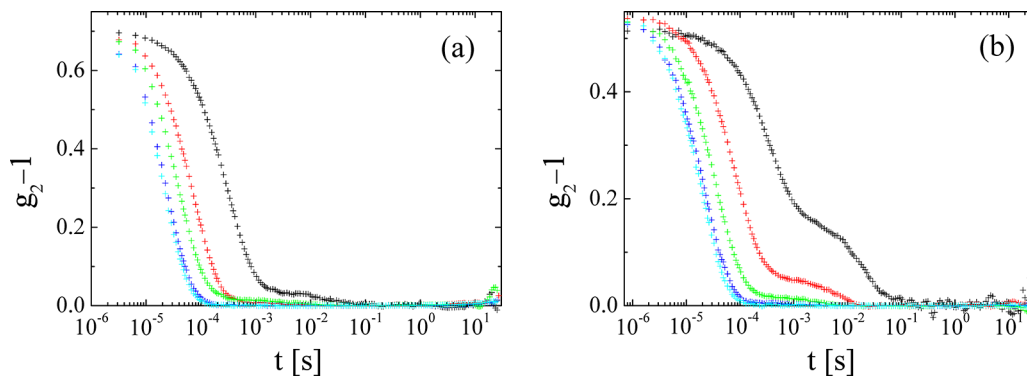

FIG. 6. (a) The DLS spectra of the 3D Ising system at 20 °C with $Q = 0.000\,49$ Å^{-1} (black), $0.000\,95$ Å^{-1} (red), $0.001\,35$ Å^{-1} (green), $0.001\,65$ Å^{-1} (blue), and $0.001\,76$ Å^{-1} (cyan). All spectra were analyzed using a single exponential function. (b) the DLS spectra of the 2D Ising system at 20 °C with the same Q and the same colors. All spectra were analyzed using two exponential functions, and only if the second exponential was negligible was it omitted.
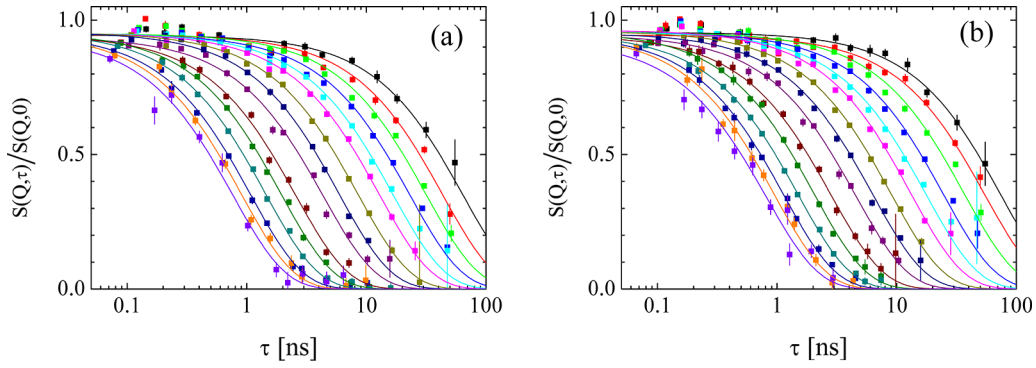
FIG. 7. (a) The NSE spectra of the 3D Ising system at 20 °C with $Q = 0.041$ Å^{-1} (black), 0.051 Å^{-1} (red), 0.060 Å^{-1} (green), 0.070 Å^{-1} (blue), 0.080 Å^{-1} (cyan), 0.090 Å^{-1} (magenta), 0.104 Å^{-1} (dark yellow), 0.121 Å^{-1} (dark blue), 0.138 Å^{-1} (dark purple), 0.162 Å^{-1} (brown), 0.181 Å^{-1} (dark green), 0.203 Å^{-1} (blue-green), 0.230 Å^{-1} (dark-dark blue), 0.249 Å^{-1} (orange), and 0.268 Å^{-1} (purple). All spectra are described with single exponential functions (solid lines, same color). (b) The NSE spectra of the 2D Ising system at 20 °C with the same Q and the same colors.

each system could be described using the modified crossover function of Kawasaki [Eqs. (5)–(7)] [42]. The fit parameters are summarized in Table IV. We used a rather experimental amplitude A with the dimension Å^z, which in theory should be $A_d = R\xi_0^z/(8\pi)$ (see Table II). The most important dependence on the dimensionality lies in the amplitude R [39], which theoretically is dominated by the dependence $R \propto \epsilon^{-1} = (4 - d)^{-1}$ (with d being the dimensionality). This dependence is well covered by our expectations. The scaling β shifts the upturn of the curve horizontally to higher $Q\xi$ according to the argument $X = \beta Q\xi$ in the crossover function [Eqs. (6) and (7)]. First of all, this experimental correction is within a limit of $2^{\pm 1}$, and so the theory can be considered as confirmed. Secondly, the NSE data also showed in previous experiments that they cross the theoretical dependence at a given fixed temperature with a different slope [58]. A different slope can be of two origins: A background contribution to the diffusion constant (which would need a negative amplitude to describe the measurements) or a short-scale cutoff due to the size of the 3MP molecules. The background contribution with negative amplitude bears conflicts with the thermal sta-

bility of the system towards low temperatures [37,59]. The short-scale cutoff correction should be rather small within the measured Q-range. So, at present, we cannot conclude about the physical origin of the shift factor β. The dynamic exponent z agrees with expectations. Other 3D Ising systems confirmed this exponent to a much higher precision [36], and we also measured the critical exponent $x = 0.042$ of the viscosity consistently. The 2D Ising exponent of approximately zero would be motivated by an older argument [40,41] with the exponent of the heat capacity α being also zero (and both exponents should be proportional to each other).

The problem of the Pomeau divergence for two dimensions is solved by the observation of the charge density waves by DLS. We summarized the diffusion constant in Fig. 9. Here, the amplitudes get extremely small when $Q\xi > 0.04$, and then the exact values cannot be obtained anymore. So we conclude that the charge density waves have a diffusion constant of $D_{CDW} = 0.1$ Å^2/ns. We compare these modes to osmotic modes of lamellar surfactant or lipid systems. Here, the repeat distance fluctuates, and enrichments of solvent can take place. In our 2D Ising system, the antagonistic salt decorates the enrichment domains of 3MP and D$_2$O that evolve due to the critical fluctuations. The charge density waves take place on large distances, much larger than the correlation length ξ. So, only the wave-fronts of the charge density waves are confining the 2D Ising system to this dimensionality. This is a rather weak confinement. So the solvent molecules of 3MP and D$_2$O start to diffuse with a random walk within the confinement. However, they can enter the third dimension at a breakout time τ_{br}, which is connected to the diffusion constant D_{CDW} according to $\tau_{br} = \xi^2 D_{CDW}^{-1}$. For an observation at a scattering vector Q, the corresponding time is $\tau_Q = Q^{-2}D_{DWQ}^{-1}$. We can
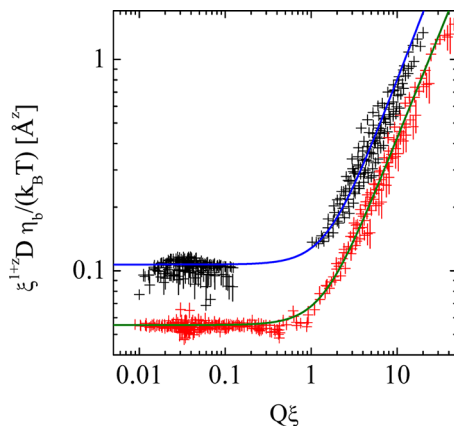

FIG. 8. The summary of the dynamic scattering experiments: the scaled diffusion constant as a function of the dimensionless length-scale $Q\xi$. The 3D Ising system is indicated by black symbols, the 2D Ising system in red. The solid lines are fit functions of Eqs. (5)–(7).

TABLE IV. The fit parameters of the Kawasaki crossover function for the dynamics experiments.

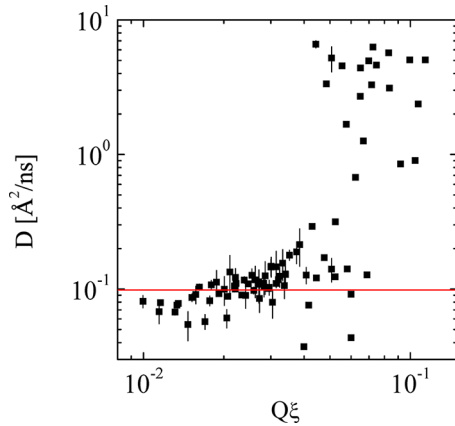| Parameter	3D Ising	2D Ising
A_d (Å^z)	0.080 ± 0.009	0.042 ± 0.004
β	0.59 ± 0.06	0.64 ± 0.06
z	0.063 ± 0.020	0.005 ± 0.019

FIG. 9. The diffusion constant of the charge density waves observed by DLS. At large $Q\xi > 0.04$, the amplitude of this mode is extremely small and so the separation of the two modes gets computationally difficult. From this experiment, we would expect a constant $D_{\text{CDW}} = 0.1$ Å^2/ns (red line).

see that these times are well above the experimental Fourier times of the NSE experiments. No charge density waves are observed in the NSE experiment due to their very low amplitudes at these large Q. The Pomeau divergence results from an integral with a kernel of $t^{-d/2}dt$ that describes the macroscopic viscosity at large times. A pure two-dimensional system would observe a logarithmic divergence. Computer simulations describe a completely different diffusion behavior at large times [38]. In our case, the integral kernel would cross over between t^{-1} and $t^{-3/2}$ at the characteristic time τ_{br}. A simple approximation would simply use τ_{br} as a cutoff in the integral. The result is a diffusion within the confinement for short times, and a more free 3D diffusion at large times. Thus, classical diffusion could be observed, and the Kawasaki crossover function could be applied to the 2D Ising system successfully.

VII. SUMMARY

After determining the static criticality of a 3D Ising and 2D Ising system made of 3MP/D$_2$O and antagonistic salt in the latter case, we observed the critical dynamics of these systems using dynamic light scattering and neutron spin echo spectroscopy. The first method focuses on the hydrodynamic modes of diffusion, while the second method observes the dynamics of the critical fluctuations. The whole experiment could be described by the modified Kawasaki crossover function. We observed the critical exponent $z = 0.06$ and $z \approx 0$, respectively. The first value is in agreement with the viscosity measurements with a critical exponent $x = 0.042$ [36]. The second value is in agreement with arguments of the exponent for the heat capacity being also zero [40,41]. The measured amplitudes of the Kawasaki crossover function differ by a factor of approx. 2. The dominating term [39], i.e., the amplitude R, is predicted to vary with the dimensionality d according to $R \propto \epsilon^{-1} = (4 - d)^{-1}$. Experimentally, we can connect this to a difference of the bare viscosity η_{b} that is approximately 1.5 times lower in the 2D case. This observations promises higher mobility of 2D confined critical fluids, which could be highly interesting for electrolytes of batteries close to the electrodes. So, after observing a higher mobility of fluids of the Brazovskii criticality close to planar surfaces (the lubrication effect [12]) [14], this observation of 2D Ising fluids correspondingly promises higher mobility close to planar interfaces.

[1] X. Hou, R. Wang, X. He, T. P. Pollard, X. Ju, L. Du, E. Paillard, H. Frielinghaus, L. C. Barnsley, O. Borodin *et al.*, Stabilizing the solid-electrolyte interphase with polyacrylamide for high-voltage aqueous lithium-ion batteries, Angew. Chem., Int. Ed. **60**, 22812 (2021).

[2] X. He, B. Yan, X. Zhang, Z. Liu, D. Bresser, J. Wang, R. Wang, X. Cao, Y. Su, H. Jia *et al.*, Fluorine-free water-in-ionomer electrolytes for sustainable lithium-ion batteries, Nat. Commun. **9**, 5320 (2018).

[3] D. Qiu, L. Peng, X. Lai, M. Ni, and W. Lehnert, Mechanical failure and mitigation strategies for the membrane in a proton exchange membrane fuel cell, Renew. Sustain. Energy Rev. **113**, 109289 (2019).

[4] D. Richter and M. Kruteva, Polymer dynamics under confinement, Soft Matter **15**, 7316 (2019).

[5] D. Noferini, O. Holderer, and H. Frielinghaus, Effect of mild nanoscopic confinement on the dynamics of ionic liquids, Phys. Chem. Chem. Phys. **22**, 9046 (2020).

[6] N. Vučemilović-Alagić, R. D. Banhatti, R. Stepić, C. R. Wick, D. Berger, M. U. Gaimann, A. Baer, J. Harting, D. M. Smith, and A.-S. Smith, Insights from molecular dynamics simulations on structural organization and diffusive dynamics of an ionic liquid at solid and vacuum interfaces, J. Colloid Interface Sci. **553**, 350 (2019).

[7] H. Weiss, J. Mars, H. Li, G. Kircher, O. Ivanova, A. Feoktystov, O. Soltwedel, M. Bier, and M. Mezger, Mesoscopic correlation functions in heterogeneous ionic liquids, J. Phys. Chem. B **121**, 620 (2017).

[8] Q. Berrod, F. Ferdeghini, P. Judeinstein, N. Genevaz, R. Ramos, A. Fournier, J. Dijon, J. Ollivier, S. Rols, D. Yu *et al.*, Enhanced ionic liquid mobility induced by confinement in 1d CNT membranes, Nanoscale **8**, 7845 (2016).

[9] S. Brazovski, Phase transition of an isotropic system to a nonuniform state, Sov. J. Exp. Theor. Phys. **41**, 85 (1975).

[10] V. Pipich, D. Schwahn, and L. Willner, Composition fluctuations in a homopolymer-diblock copolymer mixture covering the three-dimensional ising, isotropic Lifshitz, and Brasovski classes of critical universality, J. Chem. Phys. **123**, 124904 (2005).

[11] V. Pipich, L. Willner, and D. Schwahn, The ab diblock copolymer as a nonordering external field in a three-component a/b/ab polymer blend, J. Phys. Chem. B **112**, 16170 (2008).

[12] N. Gov, A. G. Zilman, and S. Safran, Hydrodynamics of confined membranes, Phys. Rev. E **70**, 011104 (2004).

[13] J. Berghausen, J. Zipfel, P. Lindner, and W. Richtering, Shear-induced orientations in a lyotropic defective lamellar phase, Europhys. Lett. **43**, 683 (1998).

[14] M. Gvaramia, G. Mangiapia, V. Pipich, M.-S. Appavou, S. Jaksch, O. Holderer, M. D. Rukhadze, and H. Frielinghaus, Tunable viscosity modification with diluted particles: When particles decrease the viscosity of complex fluids, Colloid Polym. Sci. **297**, 1507 (2019).

[15] D. A. Hajduk, H. Takenouchi, M. A. Hillmyer, F. S. Bates, M. E. Vigild, and K. Almdal, Stability of the perforated layer (PL) phase in diblock copolymer melts, Macromolecules **30**, 3788 (1997).

[16] K. Gutkowski, M. Anisimov, and J. Sengers, Crossover criticality in ionic solutions, J. Chem. Phys. **114**, 3133 (2001).

[17] M. Anisimov, S. Kiselev, J. Sengers, and S. Tang, Crossover approach to global critical phenomena in fluids, Physica A **188**, 487 (1992).

[18] K. Sadakane, N. Iguchi, M. Nagao, H. Endo, Y. B. Melnichenko, and H. Seto, 2D-Ising-like critical behavior in mixtures of water and 3-methylpyridine including antagonistic salt or ionic surfactant, Soft Matter **7**, 1334 (2011).

[19] K. Sadakane, M. Nagao, H. Endo, and H. Seto, Membrane formation by preferential solvation of ions in mixture of water, 3-methylpyridine, and sodium tetraphenylborate, J. Chem. Phys. **139**, 234905 (2013).

[20] P. Nikolai, B. Rabiyat, A. Aslan, and A. Ilmutdin, Supercritical Co_2: Properties and technological applications-a review, J. Therm. Sci. **28**, 394 (2019).

[21] V. Pipich and D. Schwahn, Densification of Supercritical Carbon Dioxide Accompanied by Droplet Formation When Passing the Widom Line, Phys. Rev. Lett. **120**, 145701 (2018).

[22] T. Narayanan and A. Kumar, Reentrant phase transitions in multicomponent liquid mixtures, Phys. Rep. **249**, 135 (1994).

[23] A. Onuki and H. Kitamura, Solvation effects in near-critical binary mixtures, J. Chem. Phys. **121**, 3143 (2004).

[24] A. Onuki, Surface tension of electrolytes: Hydrophilic and hydrophobic ions near an interface, J. Chem. Phys. **128**, 224704 (2008).

[25] D. Jung, N. Rivas, and J. Harting, How antagonistic salts cause nematic ordering and behave like diblock copolymers, J. Chem. Phys. **150**, 064912 (2019).

[26] K. Sadakane and H. Seto, Membrane formation in liquids by adding an antagonistic salt, Front. Phys. **6**, 26 (2018).

[27] D. Jung, J. Harting, and M. Sega, Monolayer structures of supramolecular antagonistic salt aggregates, J. Phys. Chem. B **125**, 2351 (2021).

[28] M. Bier, J. Mars, H. Li, and M. Mezger, Salt-induced microheterogeneities in binary liquid mixtures, Phys. Rev. E **96**, 022603 (2017).

[29] H. Tanaka, Phase separation in soft matter: The concept of dynamic asymmetry, *Soft Interfaces: Lecture Notes of the Les Houches Summer School* (Oxford University Press, Oxford, 2017), p. 465.

[30] H. Tanaka, Universality of Viscoelastic Phase Separation in Dynamically Asymmetric Fluid Mixtures, Phys. Rev. Lett. **76**, 787 (1996).

[31] L.-C. Wang, H.-S. Xu, J.-H. Zhao, C.-Y. Song, and F.-A. Wang, Density and viscosity of (3-picoline + water) binary mixtures from t = (293.15 to 343.15) k, J. Chem. Thermodyn. **37**, 477 (2005).

[32] L. Almásy, P. Banki, M. Bellissent-Funel, M. Bokor, L. Cser, G. Jancsó, K. Tompa, and J. Zanotti, Qens and nmr studies of 3-picoline–water solutions, Appl. Phys. A **74**, s516 (2002).

[33] K.-F. Tseng, T. Keller, A. C. Walters, R. J. Birgeneau, and B. Keimer, Neutron spin-echo study of the critical dynamics of spin-$\frac{5}{2}$ antiferromagnets in two and three dimensions, Phys. Rev. B **94**, 014424 (2016).

[34] H. Frielinghaus, D. Schwahn, J. Dudowicz, K. F. Freed, and K. Foreman, Small-angle neutron scattering studies of polybutadiene/polystyrene blends as a function of pressure and microstructure: Comparison of experiment and theory, J. Chem. Phys. **114**, 5016 (2001).

[35] R. F. Berg, M. R. Moldover, and G. A. Zimmerli, Viscoelasticity of Xenon near the Critical Point, Phys. Rev. Lett. **82**, 920 (1999).

[36] R. F. Berg and M. R. Moldover, Critical exponent for the viscosity of carbon dioxide and xenon, J. Chem. Phys. **93**, 1926 (1990).

[37] H. C. Burstyn, J. V. Sengers, J. K. Bhattacharjee, and R. A. Ferrell, Dynamic scaling function for critical fluctuations in classical fluids, Phys. Rev. A **28**, 1567 (1983).

[38] B. Liu, J. Goree, and O. S. Vaulina, Test of the Stokes-Einstein Relation in a Two-Dimensional Yukawa Liquid, Phys. Rev. Lett. **96**, 015005 (2006).

[39] E. Siggia, B. Halperin, and P. Hohenberg, Renormalization-group treatment of the critical dynamics of the binary-fluid and gas-liquid transitions, Phys. Rev. B **13**, 2110 (1976).

[40] M. A. Anisimov, Fifty years of breakthrough discoveries in fluid criticality, Int. J. Thermophys. **32**, 2001 (2011).

[41] P. C. Hohenberg and B. I. Halperin, Theory of dynamic critical phenomena, Rev. Mod. Phys. **49**, 435 (1977).

[42] K. Kawasaki, Decay rate of concentration fluctuation of a binary mixture in the non-hydrodynamical regime, Phys. Lett. A **30**, 325 (1969).

[43] I. D. Block and F. Scheffold, Modulated 3D cross-correlation light scattering: Improving turbid sample characterization, Rev. Sci. Instrum. **81**, 123107 (2010).

[44] M. Ohl, M. Monkenbusch, N. Arend, T. Kozielewski, G. Vehres, C. Tiemann, M. Butzek, H. Soltner, U. Giesen, R. Achten *et al.*, The spin-echo spectrometer at the spallation neutron source (sns), Nucl. Instrum. Methods Phys. Res., Sect. A **696**, 85 (2012).

[45] P. Zolnierczuk, O. Holderer, S. Pasini, T. Kozielewski, L. Stingaciu, and M. Monkenbusch, Efficient data extraction from neutron time-of-flight spin-echo raw data, J. Appl. Crystallogr. **52**, 1022 (2019).

[46] See Supplemental Material at http://link.aps.org/supplemental/10.1103/PhysRevResearch.5.023053 for the material contains Zimm plots of the SAXS curves, the critical behavior of the forward scattering, a plot of the parameter κ, and the densities of the two fluids.

[47] H. Vogel, Das temperaturabhängigkeitsgesetz der viskosität von flüssigkeiten, Phys. Z. **22**, 645 (1921).

[48] G. S. Fulcher, Analysis of recent measurements of the viscosity of glasses, J. Am. Ceram. Soc. **8**, 339 (1925).

[49] F. Hardouin, M. Achard, and G. Sigaud, Critical behaviour of dynamic twist viscosity γ_1 near polycritical points, J. Phys. Colloq. **40**, C3-371 (1979).

[50] F. Jähnig and F. Brochard, Critical elastic constants and viscosities above a nematic-smectic a transition of second order, J. Phys. France **35**, 301 (1974).

[51] A. Oleinikova, L. Bulavin, and V. Pipich, Critical anomaly of shear viscosity in a mixture with an ionic impurity, Chem. Phys. Lett. **278**, 121 (1997).

[52] M. A. Anisimov, V. A. Agayan, A. A. Povodyrev, J. V. Sengers, and E. E. Gorodetskii, Two-exponential decay of dynamic light scattering in near-critical fluid mixtures, Phys. Rev. E **57**, 1946 (1998).

[53] J. Leys, D. Subramanian, E. Rodezno, B. Hammouda, and M. A. Anisimov, Mesoscale phenomena in solutions of 3-methylpyridine, heavy water, and an antagonistic salt, Soft Matter **9**, 9326 (2013).

[54] A. F. Kostko, M. A. Anisimov, and J. V. Sengers, Criticality in aqueous solutions of 3-methylpyridine and sodium bromide, Phys. Rev. E **70**, 026118 (2004).

[55] D. Subramanian, D. A. Ivanov, I. K. Yudin, M. A. Anisimov, and J. V. Sengers, Mesoscale inhomogeneities in aqueous solutions of 3-methylpyridine and tertiary butyl alcohol, J. Chem. Eng. Data **56**, 1238 (2011).

[56] D. J. Pine, D. Weitz, J. Zhu, and E. Herbolzheimer, Diffusing-wave spectroscopy: Dynamic light scattering in the multiple scattering limit, J. Phys. France **51**, 2101 (1990).

[57] D. Richter, M. Monkenbusch, A. Arbe, and J. Colmenero, *Neutron Spin Echo in Polymer Systems* (Springer-Verlag, Berlin, Heidelberg, 2005), pp. 1–221.

[58] F. Leclercq, S. Pouget, and P. Damay, Critical slowing down in a simple fluid system as measured by neutron spin echo technique. crossover between hydrodynamics and critical dynamics, in *Neutron Spin Echo Spectroscopy: Basics, Trends and Applications* (Springer, 2002), pp. 232–245.

[59] J. K. Bhattacharjee, R. A. Ferrell, R. S. Basu, and J. V. Sengers, Crossover function for the critical viscosity of a classical fluid, Phys. Rev. A **24**, 1469 (1981).